Given a wingspan, which windplane design maximizes power?

Journal of Physics: Conference Series **2767** (2024) 072014 doi:10.1088/1742-6596/2767/7/072014

Given a wingspan, which windplane design maximizes power?

Filippo Trevisi, Alessandro Croce

Department of Aerospace Science and Technology, PoliMi, Italy

E-mail: filippo.trevisi@polimi.it

Abstract. Windplanes (i.e. Fly-Gen airborne wind energy systems) harvest wind power via the turbines placed on the tethered wing, which flies crosswind trajectories. In this paper, the optimal design of windplanes is investigated with simplified models, enabling an intuitive understanding of their physical characteristics. The windplane is then idealized as a point mass flying circular fully crosswind trajectories. If the gravity is neglected, the dynamic problem is axial symmetric and the solution is steady. The generated power can be expressed in non-dimensional form by normalizing it with the wind power passing by a disk with radius the wingspan. Since the reference area is taken to be a function of just the wingspan, looking for the design which maximizes this power coefficient addresses the question "Given a wingspan, which design maximizes power?". This is different from the literature, where the design problem is formulated per wing area and not per wingspan. The optimal designs have a finite aspect ratio and operate at the maximum lift-to-drag ratio of the airfoil. Airfoils maximizing the lift-to-drag ratio are then optimal for windplanes. If gravity is included in the model, gravitational potential energy is being exchanged over one revolution. Since this exchange comes with an associated efficiency, the plane mass and the related trajectory radius are designed to reduce the potential energy fluctuating over the loop. However, for decreasing turning radii, the available wind power decreases because the windplane sweeps a lower area. For these two conflicting reasons, the optimal mass is finite.

1. Introduction

Crosswind airborne wind energy systems (AWESs) harvest wind power by flying crosswind one or more wings, connected to the ground through a tether [1, 2]. AWESs have the potential to extract more energy at lower carbon intensity and at lower cost than established wind technologies: they are considered as one of the key technologies for the energy decarbonization [3].

Optimal design problems for fixed-wing AWESs are approached with engineering models to perform the system design, or with higher fidelity models to perform the sub-systems design. The key design metric used in the literature is the power harvesting factor [4], informing about the power per wing area. Fasel et al. [5] optimize the aerodynamic shape, compliant structure, and composite layup of a morphing wing, with the objective of maximizing the the average annual power production per wing area. Candade et al. [6] perform the aero-structural design for specific design load cases to minimize the wing mass. Bauer et al. [7] perform a system design to maximize an economic metric per wing area. Trevisi et al. [8] perform a system design to maximize the annual energy production and later the cost of energy. The wing area is fixed within an optimization, leading to optimal designs per wing area. Makani Power [9] design their Fly-Gen AWES prototype based on the power harvesting factor. Naik at al. [10, 11] study the design problem for an underwater crosswind Ground-Gen system maximizing the power and

minimizing the structural mass. The wing area is fixed within one optimization, leading to optimal designs per wing area.

In this paper, we formulate the design problem in a different way compared to the literature, by optimizing the system design per wingspan. This is similar to what is typically done for wind turbines, where the design is optimized per lifting body span and not per lifting body area. With this goal, the windplane (i.e. Fly-Gen AWES) is modeled as a point mass and we write its equations of motion in a cylindrical reference frame. We look for a periodic approximate solution of the equations of motion with a harmonic balance method, where the periodicity is driven by the gravity and the periodic control inputs. Finally, we formulate and analyze an optimal design problem, where the optimizer modifies the design variables and the control variables to maximize the mean power.

The models and the results presented in this paper are derived and analyzed in more details in the first part of the Ph.D. thesis of the first author [12].

2. Windplane point mass model

2.1. Equations of motion

Referring to Fig. 1, the ground coordinate system $\mathcal{F}_G$ is inertial and fixed at the tether attachment at the ground station. Its versor $\boldsymbol{e}_1$ points to the ground and $\boldsymbol{e}_3$ upwind. The cylindrical coordinate system $\mathcal{F}_C$, where we write the point mass equations of motion, is defined by the azimuth angle Ψ, the radial position r and the axial position z.

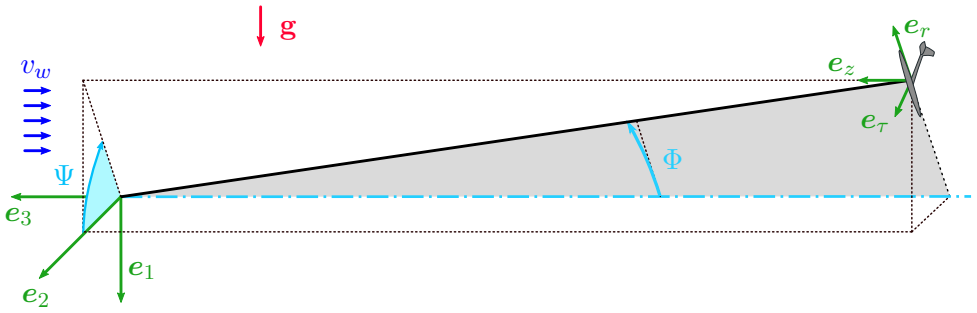

Figure 1: Ground coordinate system $\mathcal{F}_G$ and cylindrical coordinate system $\mathcal{F}_C$.

The external forces acting on the windplane are the aerodynamic force $\boldsymbol{F}_a$, the tensile force $\boldsymbol{T}$ acting on the tether and the gravitational force $m\boldsymbol{g}$. The tether tensile force $\boldsymbol{T}$ acting on the point mass is expressed as function of its axial component T_z as

$$\boldsymbol{T} = T_z \begin{bmatrix} 0 \\ -\tan\Phi \\ 1 \end{bmatrix}. \tag{1}$$

The gravitational force is $m\boldsymbol{g} = mg\,[\cos\Psi, -\sin\Psi, 0]^T$, where m is the windplane mass and g is the gravitational acceleration.

We assume here that the attitude of the windplane with respect to the wind is settled such that to be the projected crosswind area is maximized, or -in simple words- that "the windplane catches as much wind as possible". Referring to Fig. 2, the aerodynamic lift L and the parasite drag D_p are, by definition, perpendicular and parallel to the apparent velocity v_a, respectively. The onboard wind turbines thrust T_t is assumed to be parallel to the drag. The induced velocities are av_w, where a is the aerodynamic induction. The inflow angle γ is

$$\tan\gamma = \frac{v_w(1-a)}{u} = \frac{(1-a)}{\lambda}, \tag{2}$$

where λ is the wing speed ratio. The roll angle ϕ, assumed small, is used to create a lateral force. Assuming $((D_p + T_t)/L)^2 \ll 1$ and $(\tan\gamma)^2 \ll 1$, the aeordynamic force is

$$\boldsymbol{F}_a = \begin{bmatrix} L\sin\gamma - (D_p + T_t)\cos\gamma \\ (L\cos\gamma + (D_p + T_t)\sin\gamma)\phi \\ -(L\cos\gamma + (D_p + T_t)\sin\gamma) \end{bmatrix} \approx \begin{bmatrix} \frac{L}{\lambda}(1-a) - (D_p + T_t) \\ \phi L \\ -L \end{bmatrix}. \tag{3}$$

The aerodynamic lift is

$$L = \frac{1}{2}\rho A C_L u^2, \tag{4}$$

where ρ is the air density, C_L is the lift coefficient, $A = \frac{b^2}{AR}$, with AR being the wing aspect ratio, is the wing area and $v_a = u\sqrt{1 + (1/\lambda)^2} \approx u$. The aerodynamic parasite drag is

$$D_p = \frac{1}{2}\rho A C_{D,p} u^2. \tag{5}$$

$C_{D,p}$ is the parasite drag coefficient which contains not only the airfoil drag of the wing but also contributions from any other component of the airplane that is exposed to the airflow [14]. We model it as

$$C_{D,p} = \underbrace{C_{d,0} + k_d C_L^2}_{\text{airfoil polars}} + \underbrace{C_{d,te}\frac{D_{te} L_{te}}{4A}}_{\text{equivalent tether drag}}, \tag{6}$$

where $(C_{d,0}, k_d)$ model the idealized airfoil polars as function of the lift coefficient, $C_{d,te}$ is the tether profile drag coefficient, D_{te} and L_{te} its diameter and length [13]. The thrust force produced by the onboard wind turbines is

$$T_t = \frac{1}{2}\rho A_t C_{T,t} u^2, \tag{7}$$

where $C_{T,t}$ is the thrust coefficient of the onboard wind turbines with respect to the total rotor area A_t

$$A_t = n_t \cdot \pi R_t^2 = n_t \frac{\pi \xi_t^2}{4} b^2, \tag{8}$$

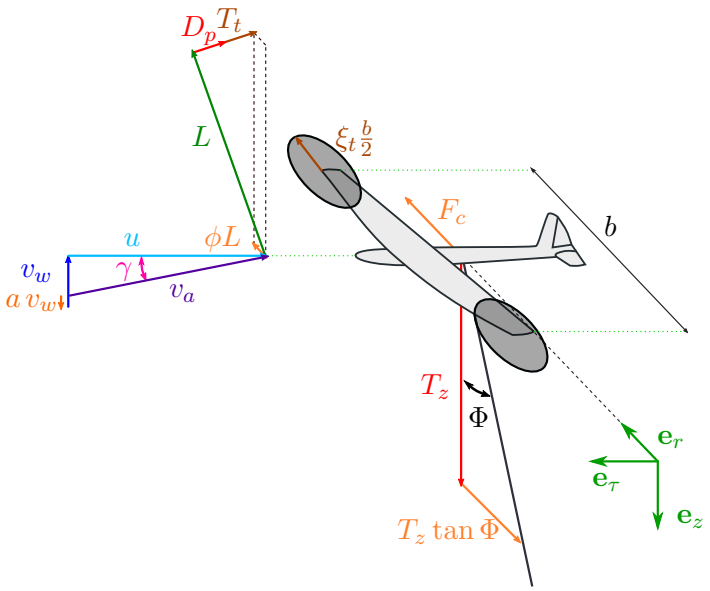

Figure 2: Velocity triangle and forces acting on a windplane in crosswind circular trajectories.

with n_t being the number of rotors of rotor radius $R_t = \xi_t \frac{b}{2}$ (Fig. 2).

Assuming a circular trajectory, the equations of motion are in equilibrium in the radial and axial direction, such that the only degree of freedom is in the tangential direction

$$\begin{cases} m\dot{u} = \frac{L}{\lambda}(1-a) - (D_p + T_t) + mg\cos\Psi \\ m\frac{u^2}{R_0} = T\tan\Phi + mg\sin\Psi - \phi L \\ T = L \end{cases} \tag{9}$$

By substituting the third equation into the second, we find an algebraic equation for the roll angle ϕ which is necessary to ensure the lateral equilibrium

$$\phi = \tan\Phi - \frac{m}{L}\frac{u^2}{R_0} + \frac{mg}{L}\sin\Psi = \tan\Phi - \frac{m}{\frac{1}{2}\rho A C_L R_0} + \frac{mg}{L}\sin\Psi. \tag{10}$$

We now take the opening angle Φ such that it compensates the second term on the right-hand-side [13]. Considering $R_0 = L_{te}\sin\Phi$, the trajectory opening angle can be found with

$$\sin\Phi\tan\Phi = \frac{m}{\frac{1}{2}\rho A C_L L_{te}}, \tag{11}$$

which does not depend on the tangential velocity because both the centrifugal forces and aerodynamic forces scale with the tangential velocity squared. The roll angle ϕ is now settled to compensate the radial component of gravity and not to turn.

The equation of motion along the tangential direction (first equation in 9) reads

$$m\dot{u} = \underbrace{\frac{1}{2}\rho A C_L u v_w}_{\text{propulsive lift}}(1-a) - \underbrace{\frac{1}{2}\rho A C_{D,p} u^2}_{\text{parasite drag}} - \underbrace{\frac{1}{2}\rho A_t C_{T,t} u^2}_{\text{turbines thrust}} + \underbrace{mg\cos\Psi}_{\text{gravity}}. \tag{12}$$

2.2. Power balance

We derive now the power balance equation by multiplying Eq. (12) with the tangential velocity u

$$m\dot{u}u = \frac{1}{2}\rho A C_L v_w u^2(1-a) - \frac{1}{2}\rho A C_{D,p} u^3 - \frac{1}{2}\rho A_t C_{T,t} u^3 + mg\cos\Psi u, \tag{13}$$

where the left-hand-side is the variation of kinetic energy. On the right-hand side, the first term is the aerodynamic power due to propulsive lift, the second the aerodynamic power dissipated in parasite drag, the third is the onboard turbines thrust power and the fourth is the gravitational power.

By normalizing the power balance in Eq. (13) with the wind power passing through a disk with radius the wingspan [16], the non-dimensional power balance is

$$\underbrace{\frac{2}{\pi}\mu\frac{b}{v_w}\dot{\lambda}\lambda}_{\frac{\partial e_k}{\partial t}} = \underbrace{\underbrace{\frac{C_L}{\pi AR}}_{C_T}\lambda^2(1-a) - \underbrace{\frac{C_{D,p}}{\pi AR}}_{C_\tau}\lambda^3}_{C_a} - n_t\frac{\xi_t^2}{4}C_{T,t}\lambda^3 + \underbrace{\frac{2}{\pi}\mu\frac{bg}{v_w^2}\lambda\cos\Psi}_{C_g}, \tag{14}$$

where $\frac{\partial e_k}{\partial t}$ is the non-dimensional change in kinetic energy, $\mu = \frac{m}{\rho b^3}$ is the non-dimensional mass, C_T is the thrust coefficient, C_τ is the parasite power coefficient, C_a the aerodynamic power coefficient and C_g the gravitational power coefficient.

The power equation can be written with respect to the onboard turbines as

$$P = \frac{1}{2}\rho A_t C_{P,t} u^3, \tag{15}$$

where $C_{P,t}$ is the power coefficient with respect to the onboard wind turbines area A_t. We define the power coefficient as the ratio the power and the wind power passing through a disk with radius the wingspan [16]

$$C_P = \frac{P}{\frac{1}{2}\rho\pi b^2 v_w^3} = C_{P,t} n_t \frac{\xi_t^2}{4}\lambda^3. \tag{16}$$

The mean value of the power balance equation over the loop is

$$\frac{1}{\mathcal{T}}\int_0^{\mathcal{T}} \frac{C_{T,t}}{C_{P,t}} C_P \, dt = \underbrace{\frac{1}{\mathcal{T}}\int_0^{\mathcal{T}} \left(C_T(1-a) - C_\tau\right) dt}_{\hat{C}_a} \tag{17}$$

where the integrals of the gravitational energy C_g and of the change of $\frac{\partial e_k}{\partial t}$ over the period are null. This equation then represents the balance between the mean aerodynamic power and the mean turbines' thrust power over the period.

The aerodynamic induction has a contribution from the near wake a_n and one from the far wake a_f [15], which is modeled as constant over the loop

$$a = a_n + a_f = \frac{C_L}{\pi AR}\lambda + \frac{\kappa_0^{\pi/2}}{4\pi}\frac{\hat{C}_T\hat{\lambda}^2}{(\hat{\lambda} - \hat{C}_T)^{3/2}}, \tag{18}$$

where $\kappa_0 = b/(2R_0)$.

3. Optimal design problem

3.1. Problem formulation

We want now to use this point mass model to formulate a high-level windplane optimal design problem. We consider the aspect ratio AR, the non-dimensional mass parameter μ and the tether diameter ratio $d_{te} = \frac{D_{te}}{b/2}$ as physical design variables. The lift coefficient C_L and the axial induction of the onboard turbines a_t (we assume momentum theory for the turbine coefficients) are the control inputs, modeled with their correspondent Fourier expansions function of the azimuth angle Ψ

$$C_L(\Psi) = \tilde{C}_L + A_{C_L,s,1}\sin\Psi + A_{C_L,c,1}\cos\Psi + A_{C_L,s,2}\sin(2\Psi) + A_{C_L,c,2}\cos(2\Psi), \tag{19}$$

and

$$a_t(\Psi) = \tilde{a}_t + A_{a_t,s}\sin\Psi + A_{a_t,c}\cos\Psi. \tag{20}$$

The design problem reads

$$\begin{aligned} \text{maximize: } & \hat{C}_P\Big(\overbrace{a_f, \boldsymbol{\Lambda}}^{\text{dependent vars}}, \overbrace{C_L(\Psi), a_t(\Psi), AR, \mu, d_{te}}^{\text{design variables}}, \overbrace{b, v_w, \xi_t, C_{d,0}, k_d, C_{d,te}, l_{te}, \overline{\sigma}_{te}}^{\text{independent variables}} \Big) \\ \text{subject to: } & [h_{a_f}; \boldsymbol{H}] = \mathbf{0} \quad \text{equality constraint} \\ & c_\sigma < 0 \quad \text{inequality constraint,} \end{aligned} \tag{21}$$

where the dependent variables are modified by the optimizer to solve the equality constraints. The axial induction due to the far wake a_f solves the far wake part of Eq. 18. The Fourier coefficients of the wing speed ratio $\boldsymbol{\Lambda}$, up to the fifth harmonic, set to zero the Fourier coefficients of the residual of the equation of motion $\boldsymbol{H}$ [17]. The inequality constraint c_σ defines the tether diameter, by sizing it according to the maximum tether strength $\overline{\sigma}_{te}$.

Note that the denominator in the power coefficient definition (Eq. 16) is just function of independent variables, so that optimizing for the mean power coefficient is equivalent to optimizing for the mean power.

3.2. Optimal designs

A realistic windplane design is carried out accounting for the power generated in a range of wind speeds. The design of a wind energy system is typically determined to maximize an economic or a performance metric. A key performance indicator is the capacity factor, determined by the wind resources and the power curve, and measuring how much energy is produced by the system compared with its rated power. For a given rated power, the plane structure is expected to be a small share of the initial capital cost. Thus, larger and larger planes can be designed, without a big impact on the total costs [8]. This is the key to lower the rated wind speed and thus to reach high capacity factors. To simplify the understanding of the results, the design of a 10 m wingspan windplane is then carried out at a wind speed representative of the rated wind speed for windplanes $v_w = 7$ m/s, lower than typical values of conventional turbines, and for the independent variables in Table 1. The airfoil parameters fit the NACA 2412 polars at $Re = 10^6$. The tether drag coefficient is taken as $C_{d,te} = 0.8$, which is representative of a cylindrical tether section. The design tether material strength $\overline{\sigma}_{te}$ is used to size the tether diameter.

Table 1: Values and description of the independent variables for the optimal design problems.

		units	Description
b	10	m	Wing span
v_w	7	m/s	Wind velocity
ξ_t	0.15	-	Non dimensional onboard wind turbines radius
n_t	2	-	Number of onboard wind turbines
$C_{d,0}$	0.004	-	Airfoil polar parameters
k_d	0.008	-	
$C_{d,te}$	0.8	-	Tether drag coefficient
l_{te}	20	-	Tether length ratio
$\overline{\sigma}_{te}$	600	MPa	Design tether material strength

We solve three optimal design problems ODPs of incremental complexity to better understand the results. The optimal designs are detailed in Table 2. The first optimal design problem, denoted with PM_S (Point mass steady), is solved by setting gravity to zero, then looking for steady solutions, and for a constant non-dimensional mass parameter $\mu = 0.1$. This is purely an aerodynamic design problem. The second optimal design problem, denoted with PM_L (Point mass light), is solved by including gravity and keeping the non-dimensional mass parameter constant to $\mu = 0.1$. The third optimal design problem, denoted with PM_H (Point mass heavy), is solved by considering the full design problem.

The power coefficient for the first two design problems is $\hat{C}_P = 1.12$ and the designs are identical. The dynamics is then not influencing the aerodynamic design problem if the mass is kept fixed. When including the non-dimensional mass among the design variables, the power coefficient improves and the optimal design slightly changes.

The design lift coefficient is found to be $\hat{C}_L \approx 0.70$ for all designs, corresponding to the maximum lift-to-drag ratio of the airfoil. We then need to use airfoils designed to maximize the lift to drag ratio. The optimal aspect ratios are finite and have low values. Keeping fixed the wingspan, high aspect ratio wings would have low induced drag but low area, leading then to a small lift force and thus small generated power. Low aspect ratio wings instead would have a large area but high induced drag, leading then to not aerodynamically efficient planes. By formulating the problem per wingspan, a finite optimal aspect ratio is then found. Note that formulating the problem per wing area, as done in the literature, leads to very high aspect ratios. Low aspect ratio designs are easier to be manufactured and meet the weight requirements. The non-dimensional mass μ for the third optimization is among the design variables and its optimal

value is finite. Depending on the independent variables, extremely light designs might be not required and the optimal mass might be obtained with cheap and sustainable materials.

Table 2: Optimal designs for the three optimal design problems.

PM_S (steady)	$\hat{C}_P = 1.12$	$\hat{C}_T = 2.96$	$\hat{C}_L = 0.70$	$\hat{\lambda} = 8.87$	$\kappa_0 = 0.13$	$a_f = 0.05$
$(AR, d_{te}) \subset \boldsymbol{dv}$	$AR = 6.0$	$\mu = 0.1$	$m = 122$ kg	$d_{te} = 1.6$ mm/m	$\hat{P} = 74.2$ kW	$\mathcal{T} = 4.0$ s
PM_L (light)	$\hat{C}_P = 1.12$	$\hat{C}_T = 2.96$	$\hat{C}_L = 0.71$	$\hat{\lambda} = 8.86$	$\kappa_0 = 0.13$	$a_f = 0.05$
$(AR, d_{te}) \subset \boldsymbol{dv}$	$AR = 6.0$	$\mu = 0.1$	$m = 122$ kg	$d_{te} = 1.6$ mm/m	$\hat{P} = 73.8$ kW	$\mathcal{T} = 4.0$ s
PM_H (heavy)	$\hat{C}_P = 1.16$	$\hat{C}_T = 3.27$	$\hat{C}_L = 0.73$	$\hat{\lambda} = 8.71$	$\kappa_0 = 0.08$	$a_f = 0.03$
$(AR, d_{te}, \mu) \subset \boldsymbol{dv}$	$AR = 5.3$	$\mu = 0.32$	$m = 390$ kg	$d_{te} = 1.8$ mm/m	$\hat{P} = 77.1$ kW	$\mathcal{T} = 6.3$ s

The wing speed ratio λ as function of the non-dimensional time $t/\mathcal{T}$ is shown in Fig. 3a for the three ODPs. The initial time corresponds to the position $\Psi = 0$, with the plane moving downwards and thus accelerating ($\dot{\Psi} < 0$, see Fig. 1). The roll angle, necessary to fulfill the radial equation of motion and maintain the circular trajectory, is shown in Fig. 3b. When the plane approaches the top part of the loop, its velocity is the lowest. To compensate the radial component of gravity (Eq. 10), the roll angle then has the largest value in the top part.

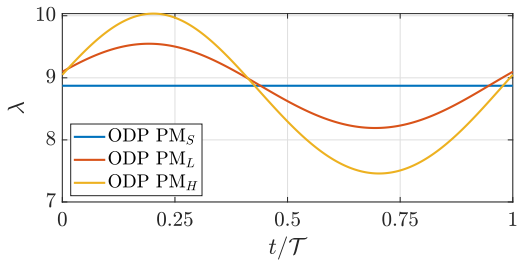

(a) Wing speed ratio λ as function of nondimensional time $t/\mathcal{T}$ for the three ODPs.

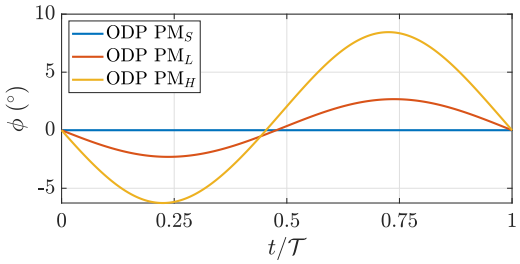

(b) Roll angle ϕ as function of non-dimensional time $t/\mathcal{T}$ for the three ODPs.

Figure 3

The onboard turbines induction a_t, thrust coefficient $C_{T,t}$ and power coefficient $C_{P,t}$ are shown as function of non-dimensional time $t/\mathcal{T}$ in Fig. 4a. In Fig. 4b, the lift coefficient as a function

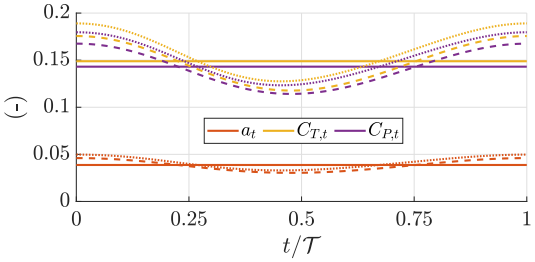

(a) Onboard turbines induction a_t, thrust coefficient $C_{T,t}$ and power coefficient $C_{P,t}$ as function of non-dimensional time $t/\mathcal{T}$ for ODP PM_S (-), ODP PM_L (- -), ODP PM_H (··).

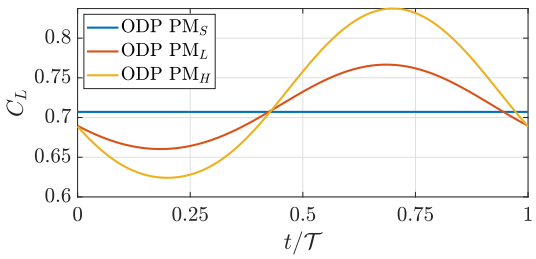

(b) Lift coefficient C_L as function of nondimensional time $t/\mathcal{T}$ for the three ODPs.

Figure 4

of the non-dimensional time is shown. The lift coefficient decreases when the plane moves downwards, and it is in phase with the wing speed ratio (Fig. 3a). The tangential component of gravity can be compensated by controlling the lift coefficient and the axial induction of the onboard turbines. Gravity has its largest value in the tangential equation of motion at $\Psi = 0$ ($t = 0$) and at $\Psi = \pi$. The lift coefficient appears out of phase with respect to gravity, while the turbines' thrust in phase. This means that the cyclic control of the turbines' thrust is aimed at compensating gravity.

The axial induction of the windplane a (Eq. 18), is shown in Fig. 5a. For all designs, it is constant over the period. The wing, which travels with a varying velocity in the circular trajectory, generates constant induced velocities. This means that the trailed vorticity is constant over the trajectory and so is the bound circulation. The power coefficient, function of $C_{P,t}$ and λ (Eq. 16), is shown in Fig. 5b.

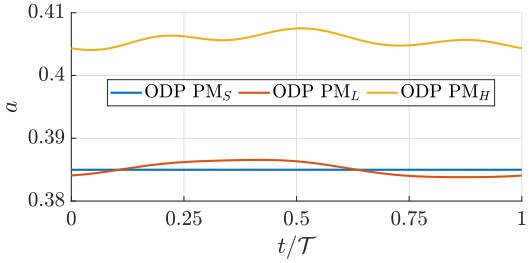

(a) Axial induction a as function of nondimensional time $t/\mathcal{T}$ for the three ODPs.

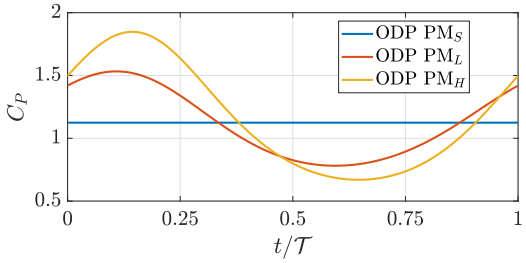

(b) Power coefficient C_P as function of nondimensional time $t/\mathcal{T}$ for the three ODPs.

Figure 5

In Fig. 6a we show the power balance for the steady ODP PM$_S$ and for the ODP PM$_L$. In the steady ODP PM$_S$, the gravitational power is not present, thus the balance is steady. The aerodynamic power $C_a = C_T(1-a) - C_\tau$ is exclusively balanced by the turbines' thrust power $\frac{C_P}{1-a_t}$. In the ODP PM$_L$, the gravitational power C_g is present and has its largest value at $\Psi = 0$ and $\Psi = \pi$. The change in kinetic energy $\frac{\partial e_k}{\partial t}$ is in phase with C_g, making the plane to accelerate. The wind power $C_T(1-a)$ and power dissipated in drag C_τ fluctuate over the PM$_S$ values.

The wing speed ratio shall be as constant as possible to minimize the power dissipated in parasite drag. To obtain a constant velocity, the onboard turbines should convert all the potential energy to electric energy, avoiding the conversion to kinetic energy. However, the potential energy converted to electric energy is reduced by the onboard generation efficiency, which decreases for increasing turbines' axial induction $\frac{C_{P,t}}{C_{T,t}} = 1 - a_t$. It is therefore optimal to let a part of the gravitational energy be converted into kinetic energy and a part into electric energy. The ratio of energy converted to kinetic and to electric is defined by the nonlinear conversion processes efficiencies.

In the ODP PM$_H$, the non-dimensional mass μ is considered among the design variables. Increasing the nondimensional mass increases the opening angle (Eq. 11), thus increases the trajectory radius and decreases the inverse turning ratio κ_0. This results in a decrease of the induction due to the far wake a_f and thus an increase in aerodynamic power. However, a larger and larger mass also increases the gravitational power C_g. The conversion of the gravitational power, as just discussed, has an associated efficiency. For these two conflicting reasons, the optimal mass, which is the main parameter determining the trajectory radius, is finite. In Fig. 6b the dependency of the power coefficient with respect to the non-dimensional mass is shown,

highlighting that the optimal mass is finite. Note that if this analysis was carried out at a lower wind speeds, the optimal mass would reduce.

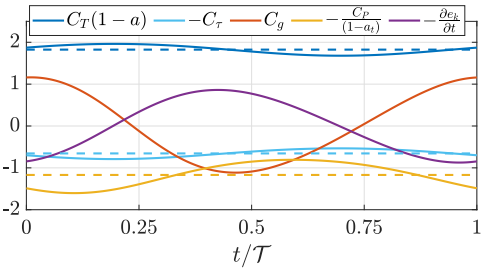

(a) Non-dimensional power balance for the steady ODP PM_S (- -) and for the light ODP PM_L (-).

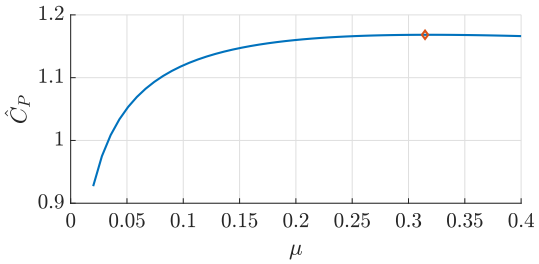

(b) Power coefficient $\hat{C}_P$ found by solving ODPs with prescribed non-dimensional mass μ.

Figure 6

In Figure 7a, the optimal power coefficients found by solving ODPs with prescribed aspect ratios are shown. The optimal aspect ratios are finite and have low values. Increasing the aspect ratio is found to be detrimental for power production. The aspect ratio can be understood as the solidity for wind turbines. Finally, the power coefficients found by solving optimal control problems with prescribed lift coefficients $\tilde{C}_L$ are shown in Fig. 7b for the light design PM_S and the heavy design PM_H. As for conventional turbines, the power coefficient is decreased when decreasing or increasing the lift coefficient with respect to the optimal value.

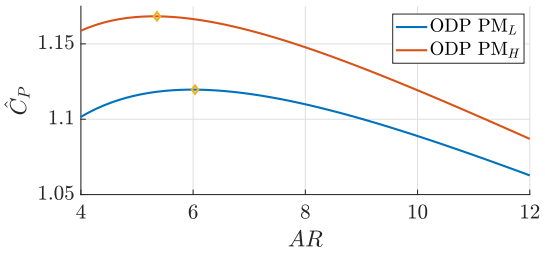

(a) Power coefficient $\hat{C}_P$ found by solving ODPs with prescribed aspect ratio AR for the optimal designs.

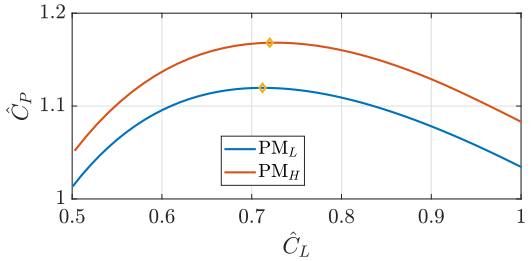

(b) Power coefficient $\hat{C}_P$ as a function of the mean lift coefficient in time $\hat{C}_L$, found by solving OCPs with prescribed $\tilde{C}_L$ for the optimal designs.

Figure 7

4. Conclusions

To study the optimal design problem, the windplane is idealized as a point mass flying circular crosswind trajectories. If gravity is removed from the model, the dynamic problem is axial symmetric and the solution is steady. In this idealized case, the power balance involves only the aerodynamic power and the turbine's thrust power. The power balance is conveniently expressed in non-dimensional form by normalizing it with the wind power passing through a disk with radius the wingspan, leading to the definition of the power and the thrust coefficients for windplanes. Since the reference area is taken to be a function of just the wingspan, looking for the design which maximizes this power coefficient is equivalent to posing the question "Given a wingspan, which design maximizes power?".

The optimal designs are obtained by operating the wing at the maximum lift-to-drag of the airfoil. Airfoils designed for high lift-to-drag ratio are used for wind turbines and shall also be

used for windplanes. The aspect ratio for windplanes has a similar physical meaning to the solidity for wind turbines. The optimal aspect ratio is finite, as the optimal solidity for wind turbines, and has a low value. If gravity is included in the model, the gravitational potential energy is being exchanged with the kinetic energy, the aerodynamic energy and the electric energy over one revolution. Since this exchange comes with an associated efficiency, the plane mass and the related trajectory are designed to reduce the potential energy fluctuating over the loop. Reducing the potential energy means reducing the turning radius and the mass. However, for decreasing turning radii, the available wind power decreases because the windplane sweeps a lower area. For these two conflicting reasons, the optimal mass is finite. Depending on the independent variables, extremely light designs might then be not required. To conclude, it is optimal to have a constant induction over the loop to maximize the raw wind power to be harvested. Therefore, the optimal lift coefficient changes according to the windplane velocity to ensure a constant intensity of the wing circulation, which translates in a constant induction.

This idealized optimization problem formulation enables the intuitive physical understanding of key physical characteristics. More analyses are presented in the first part of the Ph.D. thesis of the first author [12]. In the second part of the Ph.D. thesis, the multidisciplinary design, analysis and optimization framework T-GliDe is introduced. T-GliDe will be used to explore the design problem with more physical representation and including economic considerations in the near future.

References

[1] Loyd, M. *Crossswind Kite Power*, **Journal of Energy**, 4, 106–111, 1980.
[2] L. Fagiano, M. Quack, F. Bauer, L. Carnel, E. Oland.: *Autonomous Airborne Wind Energy Systems: Accomplishments and Challenges*. **Annual Review of Control, Robotics, and Autonomous Systems**, 5, pp. 603 – 631 (2022).
[3] M. Blanch, A. Makris, B. Valpy. *Getting airborne – the need to realise the benefits of airborne wind energy for net zero*. **Zenodo** (2022).
[4] Diehl, M.: *Airborne Wind Energy: Basic Concepts and Physical Foundations*, in: *Airborne Wind Energy*, edited by Ahrens, U., Diehl, M., and Schmehl, R., pp. 3–22, **Springer Berlin Heidelberg** (2013)
[5] Fasel, U., Keidel, D., Molinari, G., and Ermanni, P.: *Aerostructural optimization of a morphing wing for airborne wind energy applications*, **Smart Materials and Structures**, 26, 095 043, 2017.
[6] Candade, A. A., Ranneberg, M., Schmehl, R.: *Structural analysis and optimization of a tethered swept wing for airborne wind energy generation*, **Wind Energy**, 23, 1006–1025, 2020.
[7] Bauer, F., Kennel, R. M., Hackl, C. M., Campagnolo, F., Patt, M., Schmehl, R.: *Drag power kite with very high lift coefficient*, **Renewable Energy**, 118, 290–305, 2018.
[8] Trevisi, F., McWilliam, M., Gaunaa, M.: *Configuration optimization and global sensitivity analysis of Ground-Gen and Fly-Gen Airborne Wind Energy Systems*, **Renewable Energy**, 178, 385–402, 2021.
[9] Echeverri, P., Fricke, T., Homsy, G., and Tucker: *The Energy Kite Part I.*, **Makani Technologies LLC**
[10] Naik, K., Beknalkar, S., Mazzoleni, A., Vermillion, C.: *Fused Geometric, Structural, and Control design Framework for an Energy-Harvesting Ocean Kite*, in: 2021 **American Control Conference (ACC)**, pp. 3525–3531, 2021.
[11] Naik, K., Beknalkar, S., Reed, J., Mazzoleni, A., Fathy, H., Vermillion, C.: *Pareto Optimal and Dual-Objective Geometric and Structural Design of an Underwater Kite for Closed-Loop Flight Performance*, **Journal of Dynamic Systems, Measurement, and Control**, 145, 011 005, 2022.
[12] Trevisi, F., *Conceptual design of windplanes* **Ph.D. thesis**, Politecnico di Milano (2024).
[13] Trevisi, F., Gaunaa, M., Mcwilliam, Michael *The Influence of Tether Sag on Airborne Wind Energy Generation*. **Journal of Physics: Conference Series** 1618, 032006, 2020.
[14] Anderson, J. *Fundamentals of Aerodynamics.* **McGraw-Hill Education**, sixth edn., 2017.
[15] Trevisi, F., Riboldi, C. E. D., Croce, A. 2023 *Vortex model of the aerodynamic wake of airborne wind energy systems.* **Wind Energy Science** 8, 999–1016, 2023.
[16] Trevisi, F., Riboldi, C. E. D., Croce, A. *Refining the airborne wind energy systems power equations with a vortex wake model*. **Wind Energy Science** 8, 1639–1650, 2023.
[17] Trevisi, F., Castro-Fernández, I., Pasquinelli, G., Riboldi, C. E. D., Croce, A. *Flight trajectory optimization of Fly-Gen airborne wind energy systems through a harmonic balance method* **Wind Energy Science** 7, 2039–2058, 2022.